Dissipation Mechanisms in Fermionic Josephson Junction

Gabriel Wlazłowski,[1,2,*] Klejdja Xhani,[3,†] Marek Tylutki,[1,‡] Nikolaos P. Proukakis,[4,§] and Piotr Magierski[1,2,∥]

[1]*Faculty of Physics, Warsaw University of Technology, Ulica Koszykowa 75, 00-662 Warsaw, Poland*
[2]*Department of Physics, University of Washington, Seattle, Washington 98195-1560, USA*
[3]*Istituto Nazionale di Ottica del Consiglio Nazionale delle Ricerche (CNR-INO), 50019 Sesto Fiorentino, Italy*
[4]*Joint Quantum Centre (JQC) Durham-Newcastle, School of Mathematics, Statistics and Physics, Newcastle University, Newcastle upon Tyne NE1 7RU, United Kingdom*

(Received 13 July 2022; revised 10 October 2022; accepted 12 December 2022; published 12 January 2023)

We characterize numerically the dominant dynamical regimes in a superfluid ultracold fermionic Josephson junction. Beyond the coherent Josephson plasma regime, we discuss the onset and physical mechanism of dissipation due to the superflow exceeding a characteristic speed, and provide clear evidence distinguishing its physical mechanism across the weakly and strongly interacting limits, despite qualitative dynamics of global characteristics being only weakly sensitive to the operating dissipative mechanism. Specifically, dissipation in the strongly interacting regime occurs through the phase-slippage process, caused by the emission and propagation of quantum vortices, and sound waves—similar to the Bose-Einstein condensation limit. Instead, in the weak interaction limit, the main dissipative channel arises through the pair-breaking mechanism.

DOI: 10.1103/PhysRevLett.130.023003

Introduction.—The Josephson effect of a supercurrent tunneling through a weak barrier has been one of the hallmarks of superfluidity. Originally it was proposed and realized as a junction between two superconductors separated by a thin insulating barrier [1,2]. With the advent of experiments with ultracold quantum gases, one can produce a Josephson junction setup by splitting the atomic cloud into two parts through a relatively thin external potential [3–6]. Controlling the number of atoms in both reservoirs, one can produce either dc or ac Josephson junction. In the latter, the difference in chemical potentials between both clouds plays the role of dc voltage used in the electronic Josephson junctions. In such atomic systems, the tunability of interparticle interactions provides the means to controllably investigate in a single system the dynamics, and stability, of such supercurrents across the BEC-BCS crossover [7–11], including the strongly interacting unitary Fermi gas (UFG) regime, which combines properties of the two limits. Although one would expect different physical mechanisms to be at play in the limiting cases due to distinct low-lying excitation modes, understanding the dissipative dynamics in a fermionic Josephson junction across such regimes from a microscopic level remains an open question.

In this Letter, we provide clear evidence distinguishing the different physical mechanisms at play during the dynamical evolution across the junction in a testable environment, thus extending beyond the well-studied BEC regime [3,5,6,9,12–16] for which simulations are relatively easy at the mean-field (Gross-Pitaevskii) level [17]. Specifically, our numerical study—which features no adjustable parameters—is performed in the context of a highly controllable ultracold fermionic atom experiment at LENS (Florence), which observed the transition from coherently oscillating to decaying supercurrents [8]. Our time-dependent analysis unambiguously identifies the distinct microscopic origins of emerging dissipative dynamics across the weakly (BCS) and strongly (UFG) interacting limits, despite global system quantities exhibiting similar features.

Theoretical model.—The BCS regime of the superfluid Fermi gas is studied by means of the time-dependent Bogoliubov–de Gennes (BdG) equations [18]; until now, essentially all such fermionic Josephson junction studies were limited to considerations of either static cases [19–21] or 1D scenarios [22] (with a simplified two-mode model considered in Refs. [23,24]). The time-dependent BdG equations describe the evolution of quasiparticle wave functions $\varphi_n(\mathbf{r},t) = [u_n(\mathbf{r},t), v_n(\mathbf{r},t)]^T$, and the Pauli principle is manifested by orthonormality $\int \varphi_n^\dagger(\mathbf{r},t)\varphi_m(\mathbf{r},t)d\mathbf{r} = \delta_{nm}$ that must be satisfied at each time. The equations read (using units of $m = \hbar = 1$)

$$i\frac{\partial}{\partial t}\begin{pmatrix} u_n(\mathbf{r},t) \\ v_n(\mathbf{r},t) \end{pmatrix} = \begin{pmatrix} h(\mathbf{r},t) & \Delta(\mathbf{r},t) \\ \Delta^*(\mathbf{r},t) & -h^*(\mathbf{r},t) \end{pmatrix}\begin{pmatrix} u_n(\mathbf{r},t) \\ v_n(\mathbf{r},t) \end{pmatrix}, \quad (1)$$

where h is the single quasiparticle Hamiltonian $h(\mathbf{r},t) = -(\nabla^2/2) + U(\mathbf{r},t) + V_{\mathrm{ext}}(\mathbf{r},t) - \mu$ shifted by the chemical potential μ. U is the mean-field potential, which is routinely neglected in the BCS regime, and $V_{\mathrm{ext}}(\mathbf{r},t)$ is an external potential. The pairing potential $\Delta(\mathbf{r},t) = -g\nu(\mathbf{r},t)$ models Cooper pairing phenomena, where $g = 4\pi a_s$ is the coupling constant defined through the scattering length a_s, and the anomalous density reads $\nu = \sum_{E_n>0} v_n^* u_n$, where E_n is quasiparticle energy corresponding to nth quasiorbital. In practice, a renormalized coupling constant is used, with the sum evaluated up to a cutoff energy E_c in order to cure the ultraviolet divergence [25,26]. The equations are valid for $|a_s k_F| \lesssim 1$. The Fermi wave vector and associated Fermi energy are defined through relation to gas density n as $k_F = \sqrt{2\varepsilon_F} = (3\pi^2 n)^{1/3}$. In order to initialize the time-dependent simulation we need to provide the solution of the static variant of Eq. (1); i.e., we carry out the replacement $i(\partial/\partial t) \to E_n$. Our analysis is based on the following observables (omitting here, for brevity, position and time dependencies): (i) the particle number density $n = \sum_{E_n>0} |v_n|^2$, (ii) the current $\boldsymbol{j} = 2\sum_{E_n>0} \mathrm{Im}[v_n \boldsymbol{\nabla} v_n^*]$, and (iii) the pairing field (order parameter) Δ.

The UFG limit is instead modeled within the framework of the superfluid local density approximation (SLDA) [26–28]. Exploiting the concept of density functional theory, this is a well-tested extension of the BdG scheme beyond the BCS regime, allowing us to grasp the limit of strong interaction regime with $a_s k_F \to \infty$. The scale invariance property of the UFG imposes that $\Delta^{(\mathrm{UFG})} = -(\gamma/n^{1/3})\nu$, and $U^{(\mathrm{UFG})} = [\beta(3\pi^2 n)^{2/3}/2] - (|\Delta|^2/3\gamma n^{2/3})$, which is no longer negligible. The coupling constants β and γ are adjusted to ensure correct reproduction of basic properties of the uniform gas, like the Bertsch parameter $\xi_0 \approx 0.4$ and the energy gap $\Delta/\varepsilon_F \approx 0.5$. Over the years, the SLDA approach has been successfully applied to a variety of problems, like dynamics of topological defects [29–33], Higgs modes [34], properties of spin-imbalanced systems [27,35–38], and even quantum turbulence [39,40].

Parameter regime and numerical implementation.—Our studies are motivated by the LENS ^{6}Li experimental setup presented in Ref. [8]. However, as the direct numerical solution of the full 3D equations of motion (1) is beyond reach of present computing systems, we simplify the computation process by adopting an effectively two-dimensional geometry: in effect, we assume quasiparticle wave functions of a generic form $\varphi_n(\mathbf{r}, t) \equiv \varphi_n(x, y, t)e^{ik_z z}$ and approximate the full 3D harmonic oscillator potential $V_{\mathrm{ho}}(\mathbf{r}) \to V_{\mathrm{ho}}(x, y) = m\omega_x^2(x^2 + \lambda^2 y^2)/2$, with $\lambda = \omega_y/\omega_x = 148/15$ being the aspect ratio, as in the experiment. We solve the problem on a computational grid of size $N_x \times N_y \times N_z = 768 \times 96 \times 24$ (lattice spacing is $dx = 1$ and defines the numerical unit of length). The number of atoms per z plane is $N_{\mathrm{tot}}/N_z \approx 830$. Simultaneously, we adjust ω_x such that $k_F \approx 1.1$ in the trap center to ensure the BCS coherence length $\xi = k_F/\pi\Delta \gtrsim dx$, so that topological defects, like quantum vortices, can be numerically resolved. The double-well geometry of the Josephson junction is engineered by adding a Gaussian barrier $V_b(\mathbf{r}) = V_0 e^{-2x^2/w^2}$ along the x axis. The initial configuration corresponds to a slight density imbalance between the two halves of the cloud, which we achieve by adding a slight linear tilt to the potential $V_{\mathrm{t}}(\mathbf{r}) = \alpha x$, when generating a stationary solution. Then, we remove the tilt and allow the system to follow its dynamics. The number of evolved quasiparticle states is $n \approx 5 \times 10^5$, which results in solving about 10^6 of coupled and nonlinear PDEs, which we treat by high-performance computing techniques.

We investigate the dynamics of Josephson atomic junction for two interaction regimes: the BCS regime with $1/a_s k_F \simeq -1$ (which extends deeper into this regime than recent experiments [8]) and the unitary limit $1/a_s k_F \simeq 0$. Guided by previous works [9,15,16] in the BEC regime ($1/a_s k_F > 1$) we consider relatively narrow barriers of width $wk_F = 5.2$ (which corresponds to a value of $w/\xi = 4$ in the UFG and 1.6 in the BCS limit) and values of $V_0/\mu < 1$ (which, in the BEC limit, were found to maximize vortex detection likelihood). Within such parameter space, we study system dynamics as a function of two control parameters: (i) the barrier height scaled to the (mean) chemical potential V_0/μ and (ii) the initial population imbalance $z_0 \equiv z(t = 0)$, where $z(t) = [N_R(t) - N_L(t)]/N_{\mathrm{tot}}$ with N_L (N_R) the number of atoms in the left (right) reservoir. The visualization of the numerical setup is presented in Figs. 1(c) and 1(d). We have also checked that conclusions are unchanged if we compare results between regimes for fixed $w/\xi = 4$.

Dynamical regimes in a Fermi superfluid.—Investigation of the dynamical regimes is performed by studying the temporal profiles of the relative imbalance $z(t)$ and its canonically conjugated variable $\Delta\phi(t) \equiv \phi_L(t) - \phi_R(t)$ [see Figs. 1(a) and 1(b)], where $\phi_{L(R)}$ is the phase of the order parameter extracted at a point in the left (right) side of the barrier. Note that the applied frameworks conserve the total energy E_{tot} [41]. Here, we consider transfer of energy stored in the junction to other degrees of freedom. The energy stored in the junction is quantified by the sum of two terms: $[E_C N_{\mathrm{tot}}^2/8]z^2(t)$ and $E_J[1-\cos\Delta\phi(t)]$, where $E_{J(C)}$ is the Josephson (capacitive) energy [14]. The nondissipative or coherent regime is characterized by sinusoidal oscillations with constant amplitude of both the variables $z(t)$ and $\Delta\phi(t)$ [9,12,13,15,42], while dissipative dynamics is reflected by the decaying amplitude for $z(t)$. As expected, the coherent oscillations are observed in both the BCS and UFG regimes for sufficiently low z_0 or V_0/μ [black lines in Figs. 1(a) and 1(b)].

At a critical value of the barrier height or the initial imbalance, the system is expected to transition to a dissipative regime [7–9,15], characterized by a damping of the population imbalance oscillation amplitude and by the relative phase showing 2π jumps, called phase slips. In the BEC limit, such dissipative dynamics have been interpreted in terms of the generation of vortices and sound waves [9,15]. A characteristic of such dissipative dynamics is the presence of kinks in $z(t)$, due to the backflow caused by the generation of quantum vortices. Similar dissipative features, with corresponding 2π phase jumps in the relative

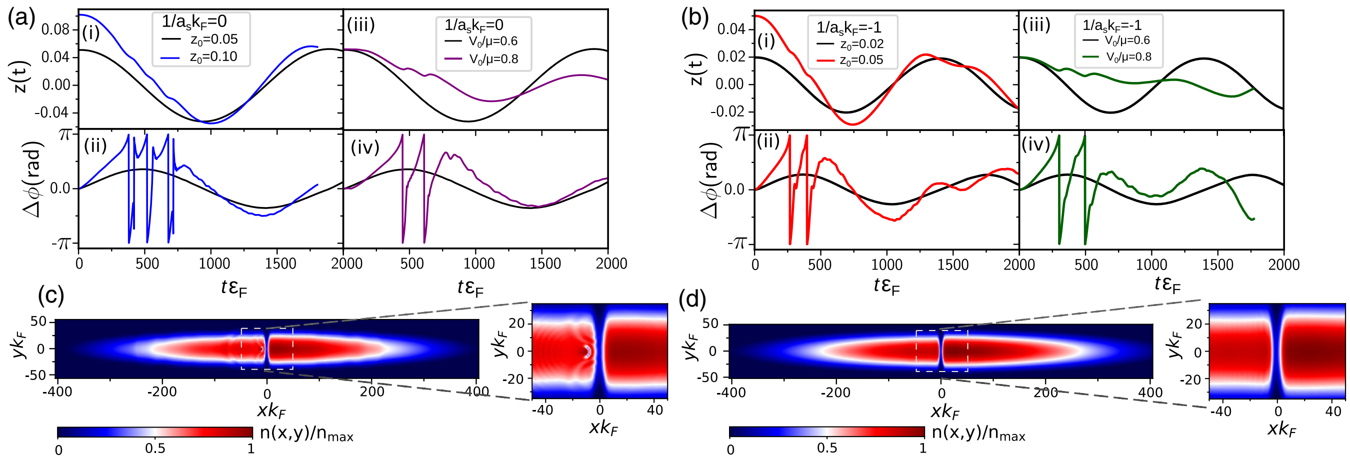

FIG. 1. Dynamical regimes for a fermionic Josephson junction. The time evolution of population imbalance $z(t)$ [(i), (iii)] and relative phase $\Delta\phi(t)$ [(ii), (iv)] in UFG (a) and BCS limit (b). The system can be driven into the dissipative regime either by increasing the value of the initial imbalance z_0 at fixed barrier height $V_0/\mu = 0.6$ (i), (ii) or by increasing the barrier strength while keeping the initial imbalance unchanged (iii), (iv). Snapshots of density distributions $n(x, y)$ (scaled to its maximum value n_{max}) at a time close to the phase-slippage event (abrupt change of $\Delta\phi$ by 2π) for UFG (c) and BCS (d), respectively. In these simulations we used $z_0 = 0.15$ and $V_0/\mu = 0.6$. The white dashed rectangular box indicates the barrier region with the enlarged plot on the right-hand side.

phase, are evidently present in the population dynamics in Figs. 1(a) and 1(b) in both the UFG and BCS limits. Despite very similar features in the above observables, a fundamental difference becomes apparent when considering the corresponding density distribution snapshot in the broader barrier region [Figs. 1(c) and 1(d)] close to the phase-slippage moment. While both vortex pairs and sound waves are found to propagate into the left reservoir in the UFG limit (being more visible for low values of V_0/μ), the corresponding BCS limit instead displays only barely visible (low amplitude) sound wave propagation and no discernible evidence of vortex generation [see also Fig. 3], a feature which is consistent across all simulations executed in the BCS regime. This points toward potentially different origin and underlying mechanisms of dissipation. Another generic feature that we find is that as we sweep the interaction from the UFG to BCS limit, for fixed barrier height V_0/μ, the critical imbalance delimiting the coherent from the dissipative regime becomes smaller. Moreover, analysis of the current-phase relation at the respective critical imbalances (at $V_0/\mu = 0.8$) reveals a lower BCS density current compared to UFG regime, consistent with the observed critical current suppression [7,8,10,43].

Dissipative mechanisms.—It is well known that matter flow can be dissipationless in the presence of an obstacle (e.g., in the form of a barrier), provided its speed does not exceed a critical value. Specifically, the Landau criterion states that if quasiparticle energy in the reference frame of the obstacle, $\varepsilon(\boldsymbol{p}) + \boldsymbol{p}\cdot\boldsymbol{v}_s$, becomes negative, then the excitations carried by this quasiparticle can be created spontaneously. Here, by $\varepsilon(\boldsymbol{p})$ we denote the quasiparticle energy of momentum $\boldsymbol{p}$ in the reference frame where the superfluid is at rest and $\boldsymbol{v}_s$ is the speed of the flow. The most common type of low-energy excitations are phonons where $\varepsilon(p) = cp$ and c is the speed of sound. The phonons can be emitted spontaneously when $v_s > c$. The speed of sound is related to the equation of state $c^2 = (\partial P/\partial n)|_S = (V^2/N)(\partial^2 E/\partial V^2)|_S$. For the UFG where $E = \xi_0 E_{\mathrm{FG}} = \xi_0 \frac{3}{5} N_{\mathrm{tot}}\varepsilon_F$, we have $c_{\mathrm{UFG}} = \sqrt{(\xi_0/3)}v_F$, where v_F is the Fermi velocity. Using BCS theory where $E = E_{\mathrm{FG}} - (3N\Delta^2/8\varepsilon_F)$ with $\Delta/\varepsilon_F = (8/e^2)e^{\pi/2a_sk_F}$, we obtain

$$c_{\mathrm{BCS}} = \sqrt{\frac{1}{3} - \frac{12}{e^4}e^{\pi/a_sk_F}\left[\left(\frac{\pi}{3a_sk_F}\right)^2 - \frac{2\pi}{3a_sk_F} + \frac{10}{9}\right]}\,v_F. \quad (2)$$

Qualitatively, the speed of sound increases as we quench the interaction toward the deep BCS regime.

Besides creating phonons, for Fermi systems we may break Cooper pairs and induce quasiparticle excitations with energy $\varepsilon(p) = \sqrt{[(p^2/2) - \mu]^2 + \Delta^2}$. Then the Landau criterion leads to a distinct critical velocity, associated with *pair breaking*, $v_{\mathrm{pb}} = \sqrt{\sqrt{\mu^2 + \Delta^2} - \mu}$. For the UFG, where $\mu/\varepsilon_F = \xi_0$ and $\Delta/\varepsilon_F \approx 0.5$, one finds $v_{\mathrm{pb}} \approx c_{\mathrm{UFG}} \approx 0.36 v_F$ [18,44], while in the BCS regime where Δ is exponentially small and $\mu \approx \varepsilon_F$, we obtain $v_{\mathrm{pb}} \approx (\Delta/2\varepsilon_F)v_F \ll c_{\mathrm{BCS}}$. Thus, we expect that the pair-breaking mechanism will be dominant in the BCS regime. The critical velocities were studied in Refs. [19,45–49].

In Fig. 2 we present the flow velocity inside the barrier, $v(t) \equiv |\boldsymbol{v}(0, t)|$, normalized to the local value of the Fermi velocity, $v_F(t) = [3\pi^2 n(0, t)]^{1/3}$, and compare it to the characteristic scales. The velocity field is extracted via $\boldsymbol{v}(\boldsymbol{r}, t) = \boldsymbol{j}(\boldsymbol{r}, t)/n(\boldsymbol{r}, t)$. If the flow remains below both the speed of sound and the pair-breaking velocity, the

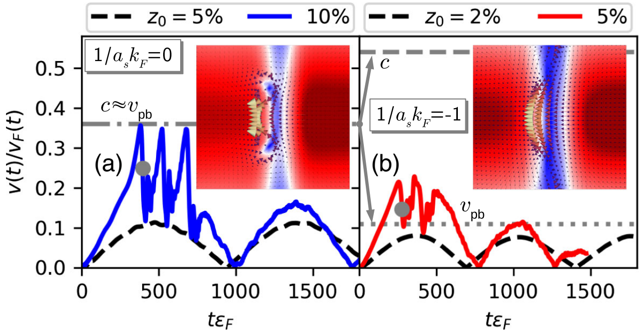

FIG. 2. The time evolution of the flow velocity in the barrier, scaled to the local Fermi velocity $v(t)/v_F(t)$ in the UFG (a) and the BCS limits (b). Dashed (black) lines demonstrate case of coherent oscillations, while solid (blue and red) lines dissipative dynamics. The gray dotted horizontal lines indicate the speed of sound c and the pair-breaking velocity $v_{\rm pb}$. These data are for fixed $wk_F = 5.2$ and fixed $V_0/\mu = 0.6$. Insets show velocity fields $\boldsymbol{v}(t)$ topology (arrows) in the barrier regions for the dissipative cases and time moments indicated by (gray) dots. The color map visualizes $|\Delta(x,y)|$. The arrows indicate separation of the scales c and $v_{\rm pb}$ in the BCS regime.

superfluid continues its motion without dissipation, oscillating coherently between the two reservoirs. However, the dynamics changes if the flow reaches one of the critical values. Consider maximum value of the flow $v_{\rm max} \equiv \max[v(t)]$. In the strongly interacting limit [Fig. 2(a)], we find that the maximal detected value is approximately equal to the speed of sound $v_{\rm max} \approx c$. Whenever the local speed approaches it, quantum vorticity is nucleated (here in the form of a vortex-antivortex pair), and the flow is reduced abruptly. Contrarily, in the BCS limit, the maximal detected speed is much lower than c, but simultaneously larger than the pair-breaking velocity $v_{\rm pb}$ calculated previously; i.e., $v_{\rm pb} \lesssim v_{\rm max} < c$. While transient configurations where the velocity field exhibits swirling patterns inside the barrier are found [inset to Fig. 2(b)], nonetheless the phase of the order parameter does not exhibit the expected topology. In other words, throughout our simulations in the BCS limit, even though the relative phase shows 2π jumps, we do not unambiguously detect winding of the phase by 2π in regions where the velocity field swirls.

The change of the dissipative mechanism becomes more evident in the case of initial imbalances z_0, much higher than the critical value. Figure 3 demonstrates the system dynamics for $z_0 = 15\%$ and 30%, while keeping other parameters as before. We observe a fast drop of $z(t)$, which starts to oscillate (irregularly) around $z = 0$. In the case of the BCS limit [Fig. 3(c)], we find that the amplitude of the residual oscillations is much smaller than in the UFG case [Fig. 3(a)], suggesting that more dissipation is present in the former case; see Ref. [41] for more details. As before, for strong interactions, we observe that quantum vortices and sound waves take away the energy to the bulk (typically the sound wave is generated due to vortex pair annihilation or during its propagation in a density gradient [9,15]). Contrary to that, in the weakly interacting case, only relatively small amplitude sound waves are observed. Such a picture is best visualized in the renormalized density carpet plots [Figs. 3(b) and 3(d)], in which the color represents the instantaneous density value along the x axis after subtracting the initial value $\delta n(x,t) \equiv n(x,0,t) - n(x,0,0)$.

In order to quantify the importance of the pair-breaking mechanism, we calculate the change in the condensation

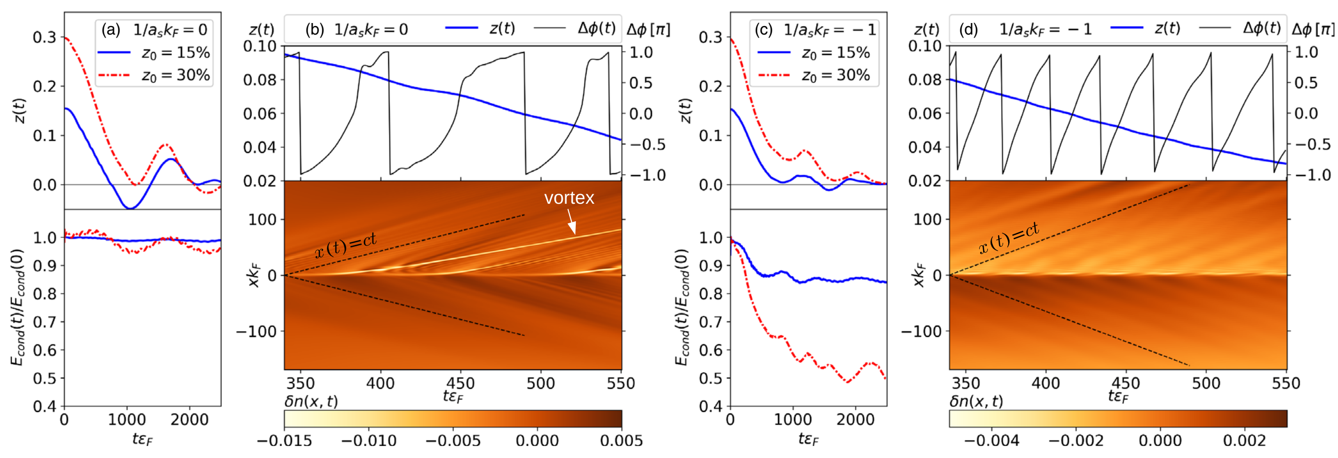

FIG. 3. The time evolution of the relative imbalance $z(t)$ (top) and the condensation energy $E_{\rm cond}(t)$ (bottom) for the unitary (a) and BCS (c) limits. The data are taken in the dissipative regimes for $V_0/\mu = 0.6$ and $wk_F = 5.2$ and for two different values of the initial imbalance z_0. For the case $z_0 = 15\%$ we show dynamics within selected time interval of the relative imbalance $z(t)$ and the relative phase difference $\Delta\phi(t)$ (top) together with the carpet plot $\delta n(x,t) \equiv n(x,0,t) - n(x,0,0)$ (bottom) for the UFG (b) and BCS (d) regimes. Dashed lines in the carpet plot indicate trajectory for objects moving with speed of sound $x = \pm ct$. In the UFG the carpet plot reveals directly both the vortex dipoles and the sound waves.

energy. According to the BCS theory, the appearance of a Cooper-pair condensate lowers the energy of the (uniform) system by $(3\Delta^2/8\varepsilon_F)N_{\rm tot}$. Using the local density approximation, we define the condensation energy for the nonuniform system as $E_{\rm cond} = \int \frac{3}{8}[|\Delta(\mathbf{r})|^2/\varepsilon_F(\mathbf{r})]n(\mathbf{r})d\mathbf{r}$. The change of $E_{\rm cond}$ is shown in the bottom panels of Figs. 3(a) and 3(c). The difference between the UFG and the BCS regimes is now evident. For the unitary gas, the condensation energy can, to good approximation, be regarded as a conserved quantity during the dynamics. Only for the most extreme case studied by us, $z_0 = 30\%$, we find that it drops by a few percent (over our probed timescale $t\varepsilon_F$). On the other hand, for the BCS gas, the energy stored in the condensate decreases noticeably in time. For example, in the analogous case $z_0 = 30\%$, we observe a drop of $E_{\rm cond}$ by about half, a striking manifestation of the depletion of the Cooper-pair condensate. It has to be noted that although the results presented above indicate the main mechanisms of energy dissipation, the accurate determination of the dissipation rate would require longer trajectories to be able to extract irreversible energy transfer.

Conclusions.—The change in the underlying physical mechanism giving rise to dissipative dynamics in Fermi superfluids from vortex nucleation to Cooper-pair breaking can be deduced based on simple arguments related to the ordering of the velocity scales c and $v_{\rm pb}$. However, it does not provide information on how this change will be manifested in the real-time (population) dynamics. Surprisingly, global characteristics like imbalance or the phase difference, which are used as primary probes in experiments, display similar patterns irrespectively of the operating mechanism. Their time dependence is similar to the experimental findings [7,8]. At unitarity, the main dissipative mechanism is related to the phase slippage, caused by emission and propagation of quantum vortices, and associated sound waves, as observed experimentally (through a barrier removal protocol which enhances vortex lifetime). Probing deeper in the BCS regime ($1/a_sk_F \simeq -1$) than is presently accessible in experiments ($1/a_sk_F \simeq -0.6$), we go beyond indirect experimental measures, such as the observed critical current suppression [8], to quantify pair breaking in terms of a decaying Cooper-pair condensation energy, finding its role to be enhanced with increasing population imbalance beyond the critical value, and to dominate the picture without any discernible direct role of vortex dynamics in this regime. In both cases, the emitted energy is ultimately converted into heat. Our Letter provides a deeper understanding of dissipation mechanisms in ultracold fermionic superfluids across the BCS-BEC crossover.

The calculations were executed by means of the W-SLDA Toolkit [50]. Detailed instructions allowing for reproduction of the presented results are given in the Supplemental Material [41]. We thank G. Roati, W. J. Kwon, and M. M. Forbes for fruitful discussions. We acknowledge PRACE for awarding us access to resource Piz Daint based in Switzerland at Swiss National Supercomputing Centre (CSCS), decision No. 2021240031. This work was supported by the Polish National Science Center (NCN) under Contracts No. UMO-2017/26/E/ST3/00428 (G. W.), No. UMO-2019/35/D/ST2/00201 (M. T.), and No. UMO-2017/27/B/ST2/02792 (P. M.), and the European Union's Horizon 2020 research and innovation programme under the Qombs project FET Flagship on Quantum Technologies GA No. 820419 (K. X.). Calculations were executed by G. W. and M. T., data analysis was performed by G. W., K. X., and M. T. All authors contributed to research planning, interpretation of the results, and manuscript writing.

*gabriel.wlazlowski@pw.edu.pl
†xhani@lens.unifi.it
‡marek.tylutki@pw.edu.pl
§nikolaos.proukakis@ncl.ac.uk
‖piotr.magierski@pw.edu.pl

[1] B. D. Josephson, Possible new effects in superconductive tunnelling, Phys. Lett. **1**, 251 (1962).
[2] B. D. Josephson, Coupled superconductors, Rev. Mod. Phys. **36**, 216 (1964).
[3] Michael Albiez, Rudolf Gati, Jonas Fölling, Stefan Hunsmann, Matteo Cristiani, and Markus K. Oberthaler, Direct Observation of Tunneling and Nonlinear Self-Trapping in a Single Bosonic Josephson Junction, Phys. Rev. Lett. **95**, 010402 (2005).
[4] C. Ryu, P. W. Blackburn, A. A. Blinova, and M. G. Boshier, Experimental Realization of Josephson Junctions for an Atom Squid, Phys. Rev. Lett. **111**, 205301 (2013).
[5] L. J. LeBlanc, A. B. Bardon, J. McKeever, M. H. T. Extavour, D. Jervis, J. H. Thywissen, F. Piazza, and A. Smerzi, Dynamics of a Tunable Superfluid Junction, Phys. Rev. Lett. **106**, 025302 (2011).
[6] S. Levy, E. Lahoud, I. Shomroni, and J. Steinhauer, The a.c. and d.c. Josephson effects in a Bose-Einstein condensate, Nature (London) **449**, 579 (2007).
[7] Giacomo Valtolina, Alessia Burchianti, Andrea Amico, Elettra Neri, Klejdja Xhani, Jorge Amin Seman, Andrea Trombettoni, Augusto Smerzi, Matteo Zaccanti, Massimo Inguscio, and Giacomo Roati, Josephson effect in fermionic superfluids across the BEC-BCS crossover, Science **350**, 1505 (2015).
[8] A. Burchianti, F. Scazza, A. Amico, G. Valtolina, J. A. Seman, C. Fort, M. Zaccanti, M. Inguscio, and G. Roati, Connecting Dissipation and Phase Slips in a Josephson Junction between Fermionic Superfluids, Phys. Rev. Lett. **120**, 025302 (2018).
[9] K. Xhani, E. Neri, L. Galantucci, F. Scazza, A. Burchianti, K.-L. Lee, C. F. Barenghi, A. Trombettoni, M. Inguscio, M. Zaccanti, G. Roati, and N. P. Proukakis, Critical Transport and Vortex Dynamics in a Thin Atomic Josephson Junction, Phys. Rev. Lett. **124**, 045301 (2020).
[10] W. J. Kwon, G. Del Pace, R. Panza, M. Inguscio, W. Zwerger, M. Zaccanti, F. Scazza, and G. Roati, Strongly correlated superfluid order parameters from dc Josephson supercurrents, Science **369**, 84 (2020).

[11] Niclas Luick, Lennart Sobirey, Markus Bohlen, Vijay Pal Singh, Ludwig Mathey, Thomas Lompe, and Henning Moritz, An ideal Josephson junction in an ultracold two-dimensional Fermi gas, Science **369**, 89 (2020).

[12] A. Smerzi, A. Trombettoni, T. Lopez-Arias, C. Fort, P. Maddaloni, F. Minardi, and M. Inguscio, Macroscopic oscillations between two weakly coupled Bose-Einstein condensates, Eur. Phys. J. B **31**, 457 (2003).

[13] A. Smerzi, S. Fantoni, S. Giovanazzi, and S. R. Shenoy, Quantum Coherent Atomic Tunneling between Two Trapped Bose-Einstein Condensates, Phys. Rev. Lett. **79**, 4950 (1997).

[14] Ivar Zapata, Fernando Sols, and Anthony J. Leggett, Josephson effect between trapped Bose-Einstein condensates, Phys. Rev. A **57**, R28 (1998).

[15] K. Xhani, L. Galantucci, C. F. Barenghi, G. Roati, A. Trombettoni, and N. P. Proukakis, Dynamical phase diagram of ultracold Josephson junctions, New J. Phys. **22**, 123006 (2020).

[16] Klejdja Xhani and Nick Proukakis, Dissipation in a finite temperature atomic Josephson junction, Phys. Rev. Res. **4**, 033205 (2022).

[17] Franco Dalfovo, Stefano Giorgini, Lev P. Pitaevskii, and Sandro Stringari, Theory of Bose-Einstein condensation in trapped gases, Rev. Mod. Phys. **71**, 463 (1999).

[18] *The BCS-BEC Crossover and the Unitary Fermi Gas*, edited by Wilhelm Zwerger (Springer, Berlin, 2012), 10.1007/978-3-642-21978-8.

[19] A. Spuntarelli, P. Pieri, and G. C. Strinati, Josephson Effect throughout the BCS-BEC Crossover, Phys. Rev. Lett. **99**, 040401 (2007).

[20] A. Spuntarelli, P. Pieri, and G. C. Strinati, Solution of the Bogoliubov–de Gennes equations at zero temperature throughout the BCS-BEC crossover: Josephson and related effects, Phys. Rep. **488**, 111 (2010).

[21] V. Piselli, S. Simonucci, and G. C. Strinati, Josephson effect at finite temperature along the BCS-BEC crossover, Phys. Rev. B **102**, 144517 (2020).

[22] Peng Zou and Franco Dalfovo, Josephson oscillations and self-trapping of superfluid fermions in a double-well potential, J. Low Temp. Phys. **177**, 240 (2014).

[23] Ji Li, Wen Wen, Yuke Zhang, and Xiaodong Ma, Josephson dynamics of strongly interacting superfluid Fermi gases in double-well potentials, Int. J. Mod. Phys. B **35**, 2150002 (2021).

[24] Ji Li, Wen Wen, Ying Wang, Xiaodong Ma, and Huijun Li, Josephson dynamics of superfluid Fermi gases in a double-well potential with dissipation or gain, Phys. Lett. A **410**, 127543 (2021).

[25] Aurel Bulgac and Yongle Yu, Renormalization of the Hartree-Fock-Bogoliubov Equations in the Case of a Zero Range Pairing Interaction, Phys. Rev. Lett. **88**, 042504 (2002).

[26] Aurel Bulgac, Local-density-functional theory for superfluid fermionic systems: The unitary gas, Phys. Rev. A **76**, 040502(R) (2007).

[27] A. Bulgac and Michael McNeil Forbes, Unitary Fermi Supersolid: The Larkin-Ovchinnikov Phase, Phys. Rev. Lett. **101**, 215301 (2008).

[28] Aurel Bulgac, Michael McNeil Forbes, and Piotr Magierski, The unitary Fermi gas: From Monte Carlo to density functionals, in *The BCS-BEC Crossover and the Unitary Fermi Gas*, Lecture Notes in Physics, edited by Wilhelm Zwerger (Springer, Berlin, 2012), pp. 305–373.

[29] Aurel Bulgac, Yuan-Lung Luo, Piotr Magierski, Kenneth J. Roche, and Yongle Yu, Real-time dynamics of quantized vortices in a unitary Fermi superfluid, Science **332**, 1288 (2011).

[30] Aurel Bulgac, Yuan-Lung Luo, and Kenneth J. Roche, Quantum Shock Waves and Domain Walls in the Real-Time Dynamics of a Superfluid Unitary Fermi Gas, Phys. Rev. Lett. **108**, 150401 (2012).

[31] Aurel Bulgac, Michael McNeil Forbes, Michelle M. Kelley, Kenneth J. Roche, and Gabriel Wlazłowski, Quantized Superfluid Vortex Rings in the Unitary Fermi Gas, Phys. Rev. Lett. **112**, 025301 (2014).

[32] Gabriel Wlazłowski, Kazuyuki Sekizawa, Maciej Marchwiany, and Piotr Magierski, Suppressed Solitonic Cascade in Spin-Imbalanced Superfluid Fermi Gas, Phys. Rev. Lett. **120**, 253002 (2018).

[33] Marek Tylutki and Gabriel Wlazłowski, Universal aspects of vortex reconnections across the BCS-BEC crossover, Phys. Rev. A **103**, L051302 (2021).

[34] Aurel Bulgac and Sukjin Yoon, Large Amplitude Dynamics of the Pairing Correlations in a Unitary Fermi Gas, Phys. Rev. Lett. **102**, 085302 (2009).

[35] Aurel Bulgac, Michael McNeil Forbes, and Achim Schwenk, Induced p-Wave Superfluidity in Asymmetric Fermi Gases, Phys. Rev. Lett. **97**, 020402 (2006).

[36] Jakub Kopyciński, Wojciech R. Pudelko, and Gabriel Wlazłowski, Vortex lattice in spin-imbalanced unitary Fermi gas, Phys. Rev. A **104**, 053322 (2021).

[37] Piotr Magierski, Buğra Tüzemen, and Gabriel Wlazłowski, Spin-polarized droplets in the unitary Fermi gas, Phys. Rev. A **100**, 033613 (2019).

[38] Piotr Magierski, Buğra Tüzemen, and Gabriel Wlazłowski, Dynamics of spin-polarized impurity in ultracold Fermi gas, Phys. Rev. A **104**, 033304 (2021).

[39] Gabriel Wlazłowski, Aurel Bulgac, Michael McNeil Forbes, and Kenneth J. Roche, Life cycle of superfluid vortices and quantum turbulence in the unitary Fermi gas, Phys. Rev. A **91**, 031602(R) (2015).

[40] Khalid Hossain, Konrad Kobuszewski, Michael McNeil Forbes, Piotr Magierski, Kazuyuki Sekizawa, and Gabriel Wlazłowski, Rotating quantum turbulence in the unitary Fermi gas, Phys. Rev. A **105**, 013304 (2022).

[41] See Supplemental Material at http://link.aps.org/supplemental/10.1103/PhysRevLett.130.023003 for technical details related to accuracy of computation, estimation of the dissipation rates, and reproduction of the results.

[42] F. Meier and W. Zwerger, Josephson tunneling between weakly interacting Bose-Einstein condensates, Phys. Rev. A **64**, 033610 (2001).

[43] M. Zaccanti and W. Zwerger, Critical Josephson current in BCS-BEC–crossover superfluids, Phys. Rev. A **100**, 063601 (2019).

[44] M. Inguscio, W. Ketterle, and C. Salomon, Ultra-cold Fermi gases, in *Proceedings of the International School of Physics "Enrico Fermi"* (IOS Press Ebooks, Amsterdam, 2007).

[45] R. Combescot, M. Yu. Kagan, and S. Stringari, Collective mode of homogeneous superfluid fermi gases in the BEC-BCS crossover, Phys. Rev. A **74**, 042717 (2006).
[46] D. E. Miller, J. K. Chin, C. A. Stan, Y. Liu, W. Setiawan, C. Sanner, and W. Ketterle, Critical Velocity for Superfluid Flow across the BEC-BCS Crossover, Phys. Rev. Lett. **99**, 070402 (2007).
[47] Wolf Weimer, Kai Morgener, Vijay Pal Singh, Jonas Siegl, Klaus Hueck, Niclas Luick, Ludwig Mathey, and Henning Moritz, Critical Velocity in the BEC-BCS Crossover, Phys. Rev. Lett. **114**, 095301 (2015).
[48] Jee Woo Park, Bumsuk Ko, and Y. Shin, Critical Vortex Shedding in a Strongly Interacting Fermionic Superfluid, Phys. Rev. Lett. **121**, 225301 (2018).
[49] Dong-Chen Zheng, Yan-Qiang Yu, and Renyuan Liao, Tuning dissipation and excitations in superfluid Fermi gases with a moving impurity, Phys. Rev. A **100**, 033611 (2019).
[50] W-SLDA Toolkit, https://wslda.fizyka.pw.edu.pl/.